ISIJ International, Vol. 58 (2018), No. 7, pp. 1210–1217

Importance of the Penetration Depth and Mixing in the IRONARC Process

Kristofer BÖLKE,[1)]* Mikael ERSSON,[1)] Matej IMRIS[2)] and Pär Göran JÖNSSON[1)]

1) KTH Royal Institute of Technology, SE-100 44 Stockholm, Sweden.
2) ScanArc Plasma Technologies AB, SE-813 21 Hofors, Sweden.

(*Received on January 24, 2018; accepted on March 27, 2018*)

One of the most important parameters for gas injection into liquid baths is the penetration depth of the gas into the bath. This is due to that it strongly influences the flow structure and hence the stirring and plume behavior in metallurgical processes.

The IRONARC process is a new energy efficient process for reduction of iron oxide to produce pig iron. The future goal is to continuously scale up the process to an industrial scale from the current pilot scale. In this process, gas is injected horizontally through a submerged nozzle into a slag bath. Hence, the penetration depth is of great importance since it greatly affect several parameters in this process. Moreover, this information is essential when scaling up the reactor from a pilot scale to an industrial scale.

In this work, the penetration depth of gas injection into water in a small scale side blown converter was studied numerically. Two different approaches with different multiphase models were tested, namely the Volume of Fluid (VOF) model and Eulerian multiphase model (EE). The penetration depth could be accurately determined for both numerical models, with a small expected deviation of 13.9% from the physical experiment results. Also, the simulation time was shorter for the Eulerian multiphase model. The penetration depth was then determined for the IRONARC pilot plant process. The results show that the plume is detached from the nozzle wall, which in turn results in a better energy usage of the gas along with a small refractory wear.

KEY WORDS: penetration depth; IronArc process; pig iron production; CO_2 reduction; ironmaking; VOF; mathematical model.

1. Introduction

Today, the blast furnace process is the most widely used process to reduce iron ore and to produce pig iron. In the steel industry, the iron ore based production is a large source of CO_2 emissions, since almost all of the iron reduction processes are coal based.[1,2)] Worldwide, the CO_2 emissions in the iron and steel industry stands for about 4% to 7% of the total world CO_2 emissions.[3)] According to another source, the World steel association, that number is 6.7%.[4)] In addition to the large amounts of emissions from the iron and steel industry, it is also the industry that consumes the largest amount of energy. Therefore, a lot of research has been made in order to reach a more energy efficient production of pig iron.[1–7)] As a result of all efforts, the pig iron production in the blast furnace have become more efficient. However, since the blast furnace still uses coke as the main energy source it is difficult to reach further reductions with respect to the CO_2 emissions.[5)]

Due to the emissions and large energy consumption during the production of pig iron in the blast furnace, the development of new technologies are of interest. One example of a new technology is the IRONARC process for a reduction of iron oxide to produce pig iron.[8)] The process exists in a small scale, but the future goal is to continuously scale up the process to an industrial scale and thereby develop an alternative to the blast furnace process. In the IRONARC process, a slag is created from material that is added in the reactor due to reactions by a gas, which is blown in at a high temperature and velocity through a plasma generator (PG). The gas is heated in the PG and then injected horizontally into the slag bath through a submerged nozzle, which is placed at the side of the reactor wall. The gas, which is a mixture of air and liquefied petroleum gas (LPG), is used for heating, stirring and as a reduction agent. The carbon monoxide that is created during the heating of the LPG, reduces the Fe_2O_3 and Fe_3O_4 contents to FeO. The last reduction from FeO to Fe is done by an addition of carbon, but this is the only step where carbon is used. All the energy used for heating comes from electricity, which gives the opportunity to use renewable resources as the primary energy source. For the existing IRONARC Pilot plant all the reduction appears in one reactor, but for the future industrial plant the reduction step will appear in two reactors. A schematic picture of the future industrial scale can be seen in **Fig. 1**. The hematite and magnetite are reduced completely by the injected gas from the PG in the first reactor and then

* Corresponding author: E-mail: bolke@kth.se
DOI: http://dx.doi.org/10.2355/isijinternational.ISIJINT-2018-043

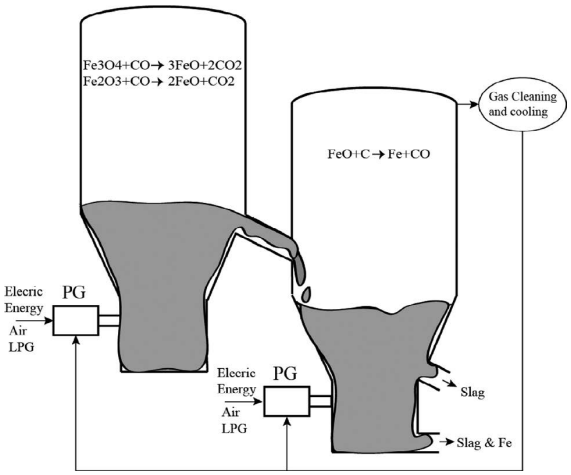

Fig. 1. Schematic figure of the future IRONARC industrial scale reactor.

the wustite is transported to the second reactor. The final reduction is done by additions of carbon. The off gas from the second reactor is cleaned, cooled and recirculated as a reducing agent which is used in the first reactor.

Due to the limitations in developing a more efficient blast furnace and the ability to reduce the CO_2 emissions along with the environmental regulations, the IRONARC process represents an interesting alternative process to the blast furnace process. If it is successfully implemented, the steel industry could take a further step into becoming a more environmentally friendly industry.

To be able to scale up the process, it is important to determine the flow pattern in the slag bath as well as the behavior of the injected gas beam. Particularly, since the injected gas is used for heating, stirring and reduction. During injection from the horizontally placed nozzle submerged under the bath, the gas will penetrate a certain distance into the bath before rising upwards in a swarm of bubbles due to buoyancy forces. This will create both stirring and mixing in the bath. The depth is referred to as the penetration depth and it greatly influences the distribution of gas bubbles in the bath and hence the flow pattern and structure of the slag bath.

The penetration depth is important to understand and to investigate since it has a major influence on the flow structure and hence the stirring and plume behavior in metallurgical processes. The IRONARC process has not been studied in the literature, since it is a new process. However, there are other metallurgical processes which use gas injection through a submerged nozzle. K. Harby[9] *et al.* investigated the penetration depth of a horizontal submerged gas jet injected into water by analyzing images captured with a high speed camera and by using two different statistical methods to evaluate the results. The author's states that the jet can be divided into two parts, namely the jet momentum part and the jet buoyant part. The results indicated that smaller Froude numbers gives larger jet oscillations at the interface and in turn smaller interface motions for higher Froude numbers. However, the Froude number seems to play a less important role for the expansion angle, where instead the nozzle diameter was of larger importance. The expansion angle was shown to increase with an increased nozzle diameter as well as with an increased flow rate.[9] Brimacombe Oryall[10] showed that the expansion angle of a submerged horizontally gas jet was 20 degrees for an air-water system and 150 degrees for a gas-mercury system. Furthermore, they found that the expansion angle does not vary significantly with the jet Froude number or the nozzle diameter. However, it was seen that the physical properties and especially the liquid density of the fluid into which the gas is injected have a strong influence on the expansion angle.

Jia-Ning Tang *et al.*[11] investigated the underwater propulsion mechanisms and showed that the main flow characteristics of gaseous jets injected into water was expansion, bulge, necking/breaking as well as back attack. These phenomena were investigated by numerical simulations of supersonic gaseous jets injected into water by using the volume of fluid (VOF) model. It was shown that these phenomena makes the flow much more unstable and turbulent, which causes the downstream pressure to fluctuate in an intense manner. Nazmul Huda *et al.*[12] investigated the penetration depth of gas in a slag-fuming furnace by using CFD simulations. These simulations of air injected into slag were validated by calculations using an empiric equation by Hoefele and Brimacombe[13] and gas injection that included combustion. Their results showed that when only gas was injected the penetration depth conformed to the equation. Furthermore, that the penetration depth was several times longer when combustion was included. An explanation for this was the increase in mass flow rate when including combustion in the simulations, since solid particles were injected together with the gas.[12] Hoefele and Brimacombe[13] studied the penetration of a horizontally injected gas jet into water, zinc chloride solution and mercury experimentally. Their results clearly showed that the penetration depth increased with an increased modified Froude number and an increased ratio of the gas density of over the liquid density. It was also shown that the gas-mercury system behaved differently than the gas-water system, due to the gas-liquid density ratio differences in the two systems. An equation for the penetration depth at the centerline of the inlet nozzle was proposed based on the experimental data. Also, Dian-Qiao *et al.*[14] investigated the flow field in a Rheinsahl-Heraeus system and proposed an equation for the penetration depth and compared the results by Hoefele and Brimacombes equation[13] and Han. It was shown that the predicted result was higher than the results of the analytical equation by brimacombe *et al.*[13] but lower than that of Han.

Odenthal *et al.*[15] investigated the penetration depth of argon gas injected into liquid steel in the AOD process by using an Euler-Euler approach, which described the injected gas and steel interface. The author also carried out water experiments and measured the penetration depth. The penetration depth in the AOD process varied between 0.35 and 0.4 m, which agreed well with the penetration depth results from the empiric relation by Hofele and Brimacombe[13] for both the water model as well as for the numerical simulation containing steel and gas. Bjurström *et al.*[16] studied the penetration depth in a side blown converter, by using physical water model experiments, at various flow rates and bath heights. It was concluded that the penetration depth is more dependent on the flow rate than the bath height. The penetration depth has also been shown to affect the wear on the refractory lining; a shorter penetration depth where the plume rises closer to the nozzle wall will increase the wear

on that particular wall. If the penetration depth is long, the wall opposing the nozzle will have an increase in refractory wear.

In this investigation two different multiphase models were tested for the estimation of the penetration depth during a submerged air injection into water and the results were compared. Then, the penetration depth in the novel IRONARC pilot plant process was investigated by using computational fluid dynamics (CFD). The Penetration depth of the IRONARC pilot plant process was investigated to be able to get an idea of the gas penetration length in the process, since this is an impossible task to investigate in the actual pilot plant process during operations.

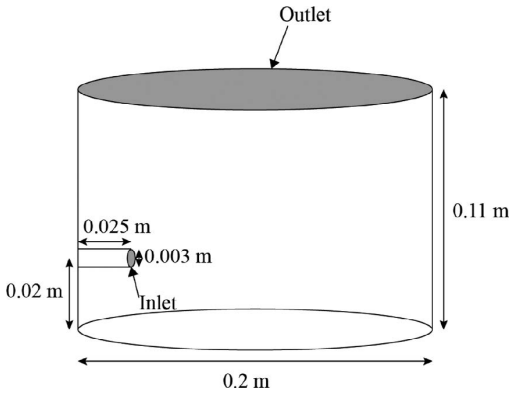

Fig. 2. Geometry of the water model domain.

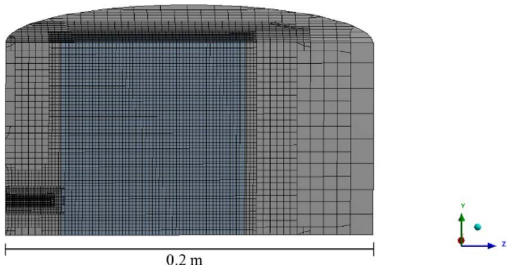

Fig. 3. Medium mesh at a cross section plane of the domain. (Online version in color.)

2. Numerical Model

2.1. Water Experiment Used for Validation

An experiment from the literature where the penetration depth was measured for pressurized air injected into water, was used as a validation for the numerical model predictions. The same parameters were used in the numerical model as in the experiment. In addition, two different numerical models were tested for estimations of the penetration depths for all three meshes. After a validation the numerical model for the penetration depth was applied on the IRONARC pilot scale process, with its geometry and parameters. Thereafter, the penetration depth for the IRONARC process was determined.

In an experiment performed by Bjurström *et al.*[16] the penetration depth of air in a small scale water model of side blown converter was measured. These data was used as validation for the numerical model predictions. In the experiment, pressurized air was blown in to a water bath through a horizontal submerged tuyere placed at the side wall of the Plexiglas model. Their experiments were performed with different bath heights and different gas flow rates. The conditions that were investigated and used for the numerical model was a bath height of 0.11 m and a gas flow rate of 800 cm^3/s. This resulted in the highest velocity of the gas at the inlet, due to no change in nozzle diameter between the different measurements. The penetration depth at these conditions was estimated to have a value of 7 cm.

2.1.1. Boundary Conditions and Solution Methods: Validation Case

All boundary conditions corresponded to the experimental procedure, where air was injected into the water from the nozzle. The speed of the air at the inlet was 113 m/s (Mach 0.33). In addition, the flow was assumed to be incompressible. In the mathematical model the volume fraction of air at the inlet exit was set to 1 and a velocity inlet was used as boundary condition for the gas injection at the inlet. At the water surface a pressure condition equal to atmospheric pressure was used. The walls were treated as stationary walls with a no-slip condition and standard wall functions were used. The geometry with the inlet and outlet boundaries of the numerical domain can be seen in **Fig. 2**.

The computational domain was created by using a 3D mainly hexahedral mesh. Three different meshes were tested for the mesh sensitivity of the domain; coarse (64000), medium (181000) and fine (350000). To reduce the computational expense for the simulations, the mesh was refined in the area of the gas plume where the interface between the phases appeared and where the velocity and volume fraction gradients were high. A cross section of the medium mesh and the refined area are shown in **Fig. 3**. The pressure-velocity coupling was solved by using the PISO algorithm. For the spatial discretization the gradients was computed by using the least square cell based method. The second order upwind scheme was chosen for momentum and first order upwind for the turbulent kinetic energy in the spatial discretization. A variable time step was used for the simulation with a global courant number of 2 for the VOF simulations.

2.2. Boundary Condition and Solution Methods, IRONARC Case

The geometry for the numerical domain was the same scale as the existing pilot plant. To reduce the simulation cost, the top part of the reactor was removed. The geometry for the IRONARC domain can be seen in **Fig. 4**. Gas was injected into the slag through a nozzle placed at the side wall. Since the injected gas consists of approximately 20 times more air than LPG, the injected gas was assumed to have the properties of air. Furthermore, the air was assumed to obtain the slag temperature momentarily. Therefore, the properties of the gas and slag were those at the temperature of 1 600°C since that is the approximate temperature of the slag. The slag was assumed to be FeO. A mass flow rate was used as a boundary condition, which corresponds to a velocity of 450 m/s. This value is below Mach 1 at this temperature and therefore it was assumed that the flow was incompressible. The gas density was constant during the simulations and the values at the operating temperature were calculated by using the ideal gas law. The simulations were performed under isothermal conditions (1 600°C).

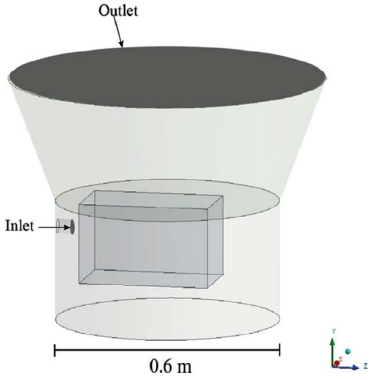

Fig. 4. Numerical domain of the IronArc pilot plant simulation. (Online version in color.)

2.3. Multiphase Theory

2.3.1. VOF Model

To describe the interface and its movement between the injected gas and the liquid phase, the volume of fluid (VOF) model was used. It tracks the interface by using a scalar quantity for the volume fraction of the phases in each cell. The continuity with VOF, which is solved for each phase, in this cases the gas and liquid, is expressed as follows:

$$\frac{\partial \alpha_q \rho_q}{\partial t} + \vec{v} \cdot \nabla \left(\alpha_q \rho_q \right) = 0 \quad \text{..... (1)}$$

where α is a scalar quantity that describes the volume fraction of the q:th phase and the constraint on which the primary phase will be computed is stated as follows:

$$\sum_{q=1}^{n} \alpha_q = 1 \quad \text{..... (2)}$$

Throughout the domain a single momentum equation is solved and the resulting velocity field is shared for the phases. The momentum equation is dependent on the volume fraction of the different phases through the viscosity and density.

$$\frac{\partial \left(\rho \vec{v} \right)}{\partial t} + \vec{v} \cdot \nabla \left(\rho \vec{v} \right) = -\nabla \mathrm{p} + \nabla \cdot \left[\mu \left(\nabla \vec{v} + \nabla \vec{v}^{T} \right) \right] + \rho \vec{g} + \vec{F} \quad \text{..... (3)}$$

The density and viscosity is calculated in each control volume as shown below:

For the density,

$$\rho = \alpha_l \rho_l + \left(1 - \alpha_l \right) \rho_g \quad \text{..... (4)}$$

and viscosity,

$$\mu = \alpha_l \mu_l + \left(1 - \alpha_l \right) \mu_g \quad \text{..... (5)}$$

where the subscripts l and g represents the liquid and gas, respectively. Due to turbulence, additional scalar equations were solved, for k and epsilon.[17,18)]

2.3.2. Eulerian Multiphase Model

For the Eulerian multiphase model the different phases are treated as interpenetrating continua and a set of equations are solved for each phase. Both phases are treated as continuous media and are averaged over each control volume. Furthermore, both continuity and momentum equations are solved for each phase and a single pressure is shared between the phases. The momentum transfer between the gas and water is modeled by using a drag term. A diameter is set for the secondary phase, which in this case is the dispersed gas bubbles. The turbulence is calculated per phase and both phases are considered to be incompressible.

The Eulerian multiphase model: The continuity equation for the Eulerian multiphase model reads as follows:

$$\frac{1}{\boldsymbol{\rho_{rq}}} \left(\frac{\partial}{\partial t} \left(\boldsymbol{\alpha_q \rho_q} \right) + \nabla \cdot \left(\boldsymbol{\alpha_q \rho_q \bar{v}_q} \right) = \sum_{p=1}^{n} \left(\dot{m}_{pq} - \dot{m}_{qp} \right) \right) \quad \text{..... (6)}$$

where $\bar{\boldsymbol{v}}_{\boldsymbol{q}}$ is the velocity of phase $\boldsymbol{q}$ and $\dot{m}_{pq}$ represents the mass transfer from the p^{th} to q^{th} phase, and $\dot{m}_{qp}$ represents the mass transfer from phase $\boldsymbol{q}$ to phase $\boldsymbol{p}$. $\boldsymbol{\alpha_q}$ is the volume fraction of phase q and $\boldsymbol{\rho_q}$ is the density of the qth phase. The parameter $\boldsymbol{\rho_{rq}}$ is the volume averaged density of the qth phase in the solution domain.

The momentum equation for phase q is as follows:

$$\begin{aligned} &\frac{\partial}{\partial t} \left(\boldsymbol{\alpha_q \rho_q \bar{v}_q} \right) + \nabla \cdot \left(\boldsymbol{\alpha_q \rho_q \bar{v}_q \bar{v}_q} \right) \\ &\quad = -\boldsymbol{\alpha_q} \nabla p + \nabla \cdot \bar{\bar{\tau}}_{\boldsymbol{q}} + \boldsymbol{\alpha_q \rho_q \bar{g}} \\ &\quad + \sum_{p=1}^{n} \left(K_{\boldsymbol{pq}} \left(\bar{\boldsymbol{v}}_p - \bar{\boldsymbol{v}}_q \right) + \dot{m}_{pq} \bar{\boldsymbol{v}}_{pq} - \dot{m}_{qp} \bar{\boldsymbol{v}}_{qp} \right) + \boldsymbol{\bar{F}_q} \end{aligned} \quad \text{... (7)}$$

where $\bar{\bar{\boldsymbol{\tau}}}_{\boldsymbol{q}}$ the q: th phase stress strain tensor, Fq is an external body force between the different phases. $\bar{\boldsymbol{v}}_{pq}$ is the interphase velocity and $\bar{\boldsymbol{g}}$ is the gravitational acceleration constant. K_{pq} is an exchange coefficient between the phases and p is the pressure shared by the phases. The general form of the K_{pq} is defined as follows:

$$K_{pg} = \frac{\rho_p f}{6 \tau_p} d_p A_i \quad \text{..... (8)}$$

where ρ_p is the density of phase p, τ_p is the particulate relaxation time, A_i the interfacial area and f is the drag function. The dragfunction is defined as follows:

$$f = \frac{C_D Re}{24} \quad \text{..... (9)}$$

where Re is the Reynolds number and C_D is the drag coefficient. In this case, the drag coefficient from the Schiller Naumann Model is used.[18–20)]

2.3.3. Turbulence Theory

The Realizable k-ε model was used to describe the turbulence in the domain:

The turbulent viscosity is calculated by combining k and e and is defined as follows:

$$\mu_t = C_\mu \frac{k^2}{\varepsilon} \quad \text{..... (10)}$$

The transport equations for k and ε are defined as follows:

$$\begin{aligned} &\frac{\partial \left(\rho k \right)}{\partial t} + \frac{\partial \left(\rho k u_j \right)}{\partial x_j} \\ &= \frac{\partial}{\partial x_j} \left[\left(\mu + \frac{\mu_t}{\sigma_k} \right) \frac{\partial k}{\partial x_j} \right] + G_k + G_b - \rho \varepsilon - Y_M + S_k \end{aligned} \quad \text{... (11)}$$

and

$$\frac{\partial(\rho\varepsilon)}{\partial t}+\frac{\partial(\rho\varepsilon u_j)}{\partial x_j}=\frac{\partial}{\partial x_j}\left[\left(\mu+\frac{\mu_t}{\sigma_k}\right)\frac{\partial\varepsilon}{\partial x_j}\right] \\ +\rho C_1 S\varepsilon-\rho C_2\frac{\varepsilon^2}{k+\sqrt{v\varepsilon}}+C_{1\varepsilon}\frac{\varepsilon}{k}C_{3\varepsilon}G_b+S_\varepsilon \quad \text{..... (12)}$$

where Gk is the production of turbulent kinetic energy due to mean velocity gradients and it is defined as follows:

$$G_k=-\rho\overline{u_i'u_j'}\frac{\partial u_j}{\partial x_i} \quad \text{..... (13)}$$

3. Results and Discussion

3.1. Validation Case, EE and VOF

The penetration depth for a side blown small scale water model was determined by using two different numerical models; namely an Eulerian multiphase (EE) model and a VOF model. A mesh analysis was made for each model and the two model predictions were compared. The models had the same boundary conditions and the same meshes were used. The simulation time for the penetration depth was 1.2 seconds; this particular time was chosen so to that the penetration depth had reached its final value with only small periodic variations in the penetration depth direction. The penetration depth (or length) has been studied several times earlier by numerical modeling; both for top blown[17,21,22] and submerged injection.[15,23,24] The VOF model is a frequently used multiphase model for this purpose,[15,23,24] while the Eulerian multiphase model is not used so frequently. However, there are cases where the Eulerian multiphase model have been used to determine the penetration depth of a horizontal gas injection.[12] Also, the definition of the penetration depth differs in different investigations. In some cases, the penetration depth is defined as the farthest depth from the injecting nozzle (in any vertical position of the plume) where the gas volume fraction drops below 80%.[12,25] In other cases, the penetration depth is defined as the farthest distance the injected gas reaches along the nozzle centerline.[16] Since the penetration depth in the experiment was measured along the nozzle centerline, the definition used for this simulation was the distance along the nozzle centerline measured from the nozzle wall to a distance where the volume fraction is 80%. If no node along the centerline for the different meshes were positioned at the exact distance where the injected air reached a volume fraction of 80%, the distance was determined by an interpolation between the closest nodes for each validation case. The gas plume in the water can be seen in **Figs. 5** and **6** for each model, respectively. These figures is an illustration of the different plume appearances between the models, but do not show the penetrated length of the gas plumes.

In **Figs. 7** and **8**, the volume fraction of air as a function of the distance from the inlet along the center line of the nozzle is shown after 1.2 seconds of injection for the EE and VOF cases, respectively. **Figures 9** and **10** shows a contour plot of the EE and VOF for the medium mesh, respectively. These figures are also after 1.2 s of flow time. The fluctuations in the bath was tested for the coarse mesh. The results showed that the penetration depth was basically

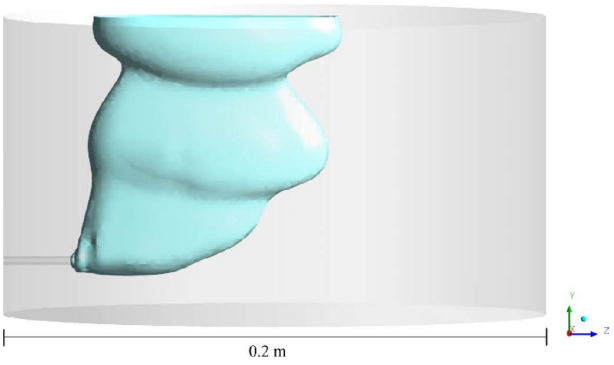

Fig. 5. Isosurface of the air plume in water for the EE-simulation. (Online version in color.)

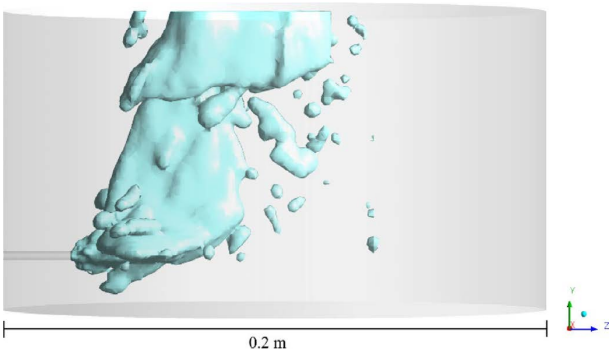

Fig. 6. Isosurface of air plume in the water for the VOF-simulation. (Online version in color.)

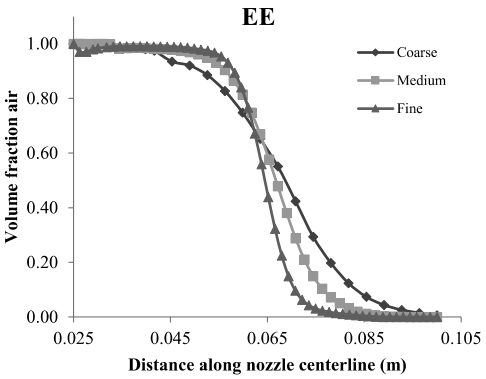

Fig. 7. Volume fraction of air as a function of distance along the nozzle centerline for EE-simulation.

the same even after approximately 20 seconds of injection and that the flow in the tank had reached some sort of steady state. The maximum time fluctuation of the velocity in this case was only a couple of mm/s for a fixed point in the water. For the EE model (Figs. 7 and 9), it can be seen that the gas plume penetrates some distance into the bath before it starts to break up and forms a mixed region, containing both gas and liquid. It is clear that the mixed region starts earlier for the coarse mesh compared to the medium and fine meshes. The sharpest interface between gas and liquid is shown for the fine mesh followed by the medium mesh and finally the coarse mesh. However, the penetration depths for the medium and fine meshes lies close to each other, with a maximum deviation of just below 3%. The deviation between the coarse and medium mesh is as large as approximately 10%. Numerical diffusion is one contribut-

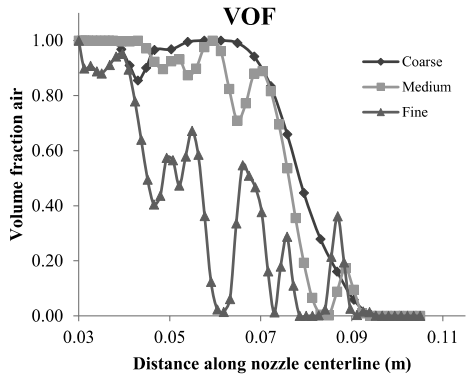

Fig. 8. Volume fraction of air as a function of distance along the nozzle centerline for VOF-simulation.

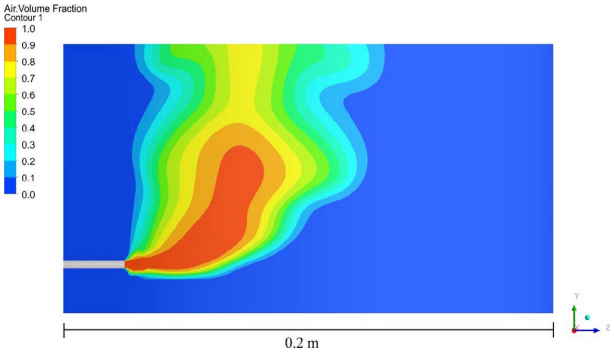

Fig. 9. Volume fraction of air for EE-model in an yz-plane located in the center of the domain. (Online version in color.)

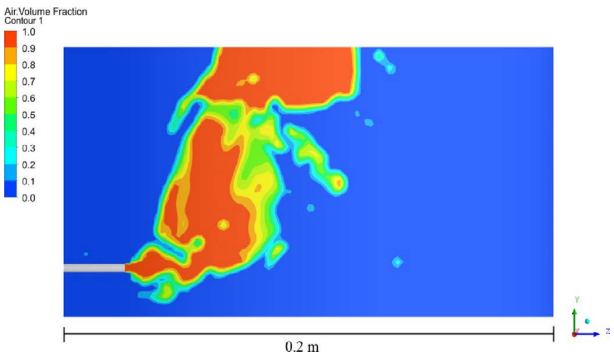

Fig. 10. Volume fraction of air for VOF-model in an yz-plane located in the center of the domain. (Online version in color.)

ing factor for the coarse mesh results, where the incline of the line that shows that the air volume fraction is quite flat compared to both the medium and fine meshes. This leads to a smearing of the gas water interface. It should also be noted that the further away from the inlet the air reaches for the different meshes, the line inclination seems to get flatter. The reason for this could be that further away from the inlet the air travels both in the vertical and horizontal direction, which is due to the results from both the momentum of the jet and the buoyancy of the bubbles. This gives the grid an inclined alignment to the air flow, which in turn increases the amount of diffusion. This phenomenon of a grid with an inclined alignment to the flow and an increase in numerical diffusion is very well known.[26] In light of the experimental results and uncertainties, both the medium and fine meshes are satisfactory to use to model the gas penetration. The simulation time for the EE simulations was approximately 1 day, 3–4 days and 1 week for the coarse, medium and fine meshes, respectively.

For the VOF simulations, the results are a lot more scattered compared to the EE simulations. As can be seen in Figs. 8 and 10, the volume fraction of the injected air does not follow the same pattern as for the EE simulations. The latter shows a clear trend of a sharper decline of the volume fraction of air further away from the nozzle compared to closer to the nozzle. As the amount of cells increase, the volume fraction value fluctuates more along the measured line. When the mesh gets finer and the number of cells increases, the plume shape becomes more irregular and more bubbles are formed. This can be seen in Fig. 8, where the volume fractions for the gas plumes for all meshes is shown. The data shows different plume shapes and an increase in the amount of bubbles as the mesh is refined. Due to this formation of bubbles large fluctuations in the air volume fraction appears. This is due to that the bubbles may be slightly off-centered compared to the line where the volume fraction is plotted. This result in a more irregular shape of the plume at the centerline, where not only gas, but also areas with water are present along the line. Due to this it is difficult to determine the penetration depth by only observing the results in Fig. 8. The criteria or definition of the penetration depth for a 80% volume fraction does not give a completely valid description of the penetration depth for the fine mesh. This is due to that according to the definition the penetration depth would be 3.7 centimeters, which clearly is not the case when observing the results in Fig. 10. The actual penetration depth is longer, but with the current definition it becomes difficult to estimate how much longer. This is due to the formation of more bubbles because of the finer discretization of the mesh. For this kind of bubbly plume maybe a plane gives a better representation than a line or a measurement over time due to this irregular bubble movement. It should be noted that the VOF model is not a bad model to simulate the plume penetration, but it requires long simulation times. Therefore, the EE model can be used to accurately describe the penetration depth at a lower computational expense.

In **Table 1**, the penetration depth for the coarse, medium and fine meshes for both the EE and VOF simulations are shown after a flow time of 1.2 s. For the medium and coarse meshes the EE simulation gave shorter penetration depths than the VOF simulations. For the latter, the penetration depths for the VOF were almost the same for the medium and coarse meshes, with a difference that was less than 1% when comparing the two meshes. For the EE simulations, there was a clear increase of 4.8% in PD between the coarse and medium mesh. Furthermore, there were basically no difference between the medium and fine meshes, where the medium mesh showed a penetration depth that was 99.8% of that of the fine mesh. However there is a large difference for the PD between the fine and medium meshes in the VOF simulations, where the penetration depth of the fine mesh is almost half the length than that of the medium mesh. As described above this is not the real penetration depth, but rather a consequence of a more irregular shaped plume that contains more bubbles. Thus, the simulations are not as accurate as the PD measurements, when measuring along a

Table 1. Simulation constants used for the fluids and in the realizable k-ε turbulence model.

Media	properties	Parameters used in the turbulence model
Air	$\rho = 1.225\ kg\ m^{-3}$	$C_\mu = 0.09$
		$C_{\varepsilon 1} = 1.44$
	$\mu = 1.7894{\cdot}10^{-3} Pa{\cdot}s$	$C_{\varepsilon 2} = 1.90$
Water	$\rho = 998.2\ kg\ m^{-3}$	$\sigma_k = 1$
		$\sigma_\varepsilon = 1.2$
	$\mu = 1.003{\cdot}10^{-3} Pa{\cdot}s$	

line with the used definition. When comparing both model results, the penetration depths of the EE simulations seems to be around 6 cm (with no difference in PD values between the medium and fine meshes) and more difficult to determine for the VOF simulations. However, the gas penetrates slightly longer for the VOF simulations if it is considered that air is present, even though it is slightly offset in position compared to the measured line. The PD for the VOF simulation could be determined by measuring the volume fraction of air along this line over time and to determine an average value of penetration depth. It is possible that this would give a better representation and a clearer PD distance value. The penetration depth of 6 cm for the EE simulation is close to the corresponding experimental penetration depth of 7 cm. The PD of the numerical simulation is based on a definition of the volume fraction that earlier has been applied by several authors.[25,26] However, it seems that the value 0.8 of the volume fraction of gas is a rather arbitrary definition without a clear description of why it was used. The experimental value was estimated and measured visually by observing and studying recorded films of the penetration of the gas in the water. This indicates that time-averaged data is appropriate to use when comparing numerical results to the experimental results. Consequently, a small deviation between the penetration depth of the experimental value and the simulation is expected.

Another thing that is to be considered is the simulation time. Here, the VOF simulations are longer than the EE simulations, when the corresponding meshes are compared. A comparison of the simulation time for the coarse mesh showed that the simulation time of the EE simulation was 10% of that of the VOF simulation. These observations do not mean that the VOF is an inaccurate model to use for the determination of the penetration depth during gas injection into a liquid. The VOF model has successfully been used in earlier investigations of the PD, but in the present case the EE simulation gives a good representation of the penetration depth in a shorter time. The Eulerian multiphase model have often been considered to be the multiphase model that is the most complex of the existing multiphase models and that has a high computational expense.[18] This is due to the strong coupling between the phases and the available interaction terms, which makes it possible to include a lot of forces of the secondary phase. Also, the EE model solves a set of equations per phase. But all interaction parameters and forces are not necessary to include for every case. Obviously there is a clear difference between investigating a single air bubble rising in water compared to a stirred water bath containing a lot of bubbles. Since not all interaction parameters have been considered in this EE-simulation, the simulation time was greatly reduced. Compared to the VOF-simulations it was also possible to use a much larger timestep, $1e^{-4}$ instead of around $5e^{-6}$. However, the predictions still gave a good representation of the penetration depth of the air injection in the water.

3.2. IRONARC

The penetration depth of the IRONARC pilot plant was determined and the gas plume that rises through the slag can be seen in **Fig. 11**, which shows the volume fraction of gas in the slag. The calculated penetration depth was estimated to approximately 0.3 m, which means that the gas travels half the distance of the diameter of the bottom cylinder of the reactor. It can be seen in the figure that the plume rises close to the nozzle wall, without being in contact with it at the center plane. If the penetration depth is too short and the gas plume rises at the nozzle wall it can result in the destruction of the freeze lining in the IRONARC reactor. Moreover, it can require that additional cooling may be needed to keep the freeze lining intact. This in turn, would result in a higher energy consumption. It will also result in a less effective energy usage, since some part of the gas will use its energy to heat the wall instead of the slag. Since the simulation shows that the gas plume rises just a couple of centimeters from the wall, the results indicates that there will be extra wear on the refractory lining compared to a longer penetration depth. The penetration depth should be long enough so that the gas bubbles are distributed throughout the slag bath and also so that the mixing is efficient, since mixing plays a major part in the process.

Accurate modelling of the penetration depth is very important for the future upscaling as well. The future reactor for the industrial process will be much larger, both with respect to the amount of charged slag and vessel dimensions. For the mixing properties in this pilot plant reactor the penetration depth is sufficient, due to that gas is distributed well within the slag bath. However, it will be shorter compared to the diameter of the larger future reactor. This is because the upscaling is limited by the gas flow rate that can pass through an individual plasma generator. Thus, instead of increasing the size of the plasma generator, the up-scaled reactor will use a larger number of plasma generators. It was also shown that the initial penetration is longer than the depth after some time when the injection of the gas has been somewhat stabilized. The fluctuations in penetration depth is greater for the gas-slag system compared to the air-water system. This might be due to the much greater density difference between the gas and liquid in the gas-slag system. Overall, the penetration depth calculations gives no indications that discourage the upscaling of the reactor. Ongoing work is done to investigate the mixing time in the system in order to judge the feasibility of the new IRONARC technology.

4. Conclusions

The penetration depth in the IronArc process has been investigated and determined numerically. In addition, model

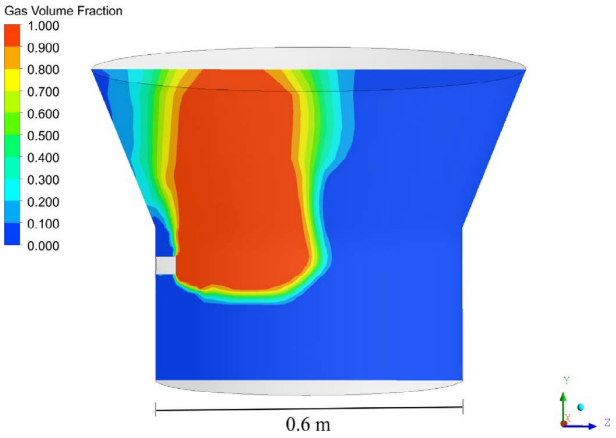

Fig. 11. Volume fraction of gas for pilot scale-model in an yz-plane located in the center of the domain. (Online version in color.)

Table 2. Number of cells, flow time and penetration depth for three meshes tested for both the EE and VOF models.

Name	Multiphase model	Mesh	Number of cells	Penetration depth (m)
Mesh 1	EE	Coarse	64000	0.058
	VOF	Coarse	64000	0.068
Mesh 2	EE	Medium	181000	0.060
	VOF	Medium	181000	0.067
Mesh 3	EE	Fine	350000	0.060
	VOF	Fine	350000	0.037
Experimental	–	–	–	0.070

validations were made of an air-water system. Two different multiphase models were tested, namely the VOF model and Eulerian multiphase model. The penetration depth for the two different set ups, with different multiphase models, were determined for three different meshes (coarse, medium and fine). Overall, the main conclusions may be summarized as follows:

- The penetration depth of the experimental air water system could be described accurately by using both the EE and VOF models. However, for the finest mesh of the VOF simulation, the fine grained multiphase structure compared to the coarse and medium meshes made it more difficult to measure the penetration depth along the nozzle centerline. This is due to a more irregular plume and due to that more bubbles are formed.
- The penetration depth of the EE corresponded to the experiments within 86%. This is a penetration depth that was very close to and just slightly smaller than the physical experiment and gave a good description of the penetration of the air in the water. Especially since it is measured at an instant of time, while the experiment all data were time averaged.
- The definition of an 80% volume fraction of gas along the nozzle centerline is a definition that describes the penetration depth for the EE simulation in an accurate way.
- After 1.2 seconds, the flow in the water had reached some sort of steady state for the simulations, when using a coarse mesh and the EE model. This is due to that the velocity fluctuations in the water for the coarse mesh were very small.
- For the air-water system, the simulation time of the EE simulation is clearly shorter than the VOF model, when the corresponding meshes are compared. A comparison showed that the EE simulation had a simulation time that was 10% of that of the VOF simulation, when the simulation time of the coarse meshes was compared. This is due to that a longer time step could be used, $1e^{-4}$ instead of around $5e^{-6}$.
- The penetration depth of the gas-slag system (IRONARC pilot plant) was calculated to have a value of approximately half the length of the reactor diameter (0.6 m). This results in an efficient distribution of gas in the slag, which is important since it enhances the mixing and makes the bubbles reach large parts of the slag.

Acknowledgements

The Authors wish to thank the Swedish Energy Agency for the financial support of this study. Also, the employees at ScanArc for their valuable help and hospitality during the visits in the facility of the pilot plant in Hofors, Sweden.

REFERENCES

1) H. Sandberg, R. Lagneborg, B. Lindblad, H. Axelsson and L. Bentell: *Scand. J. Met.*, **30** (2001), 420.
2) D. Gielen: *Energy Convers. Manag.*, **44** (2003), 1027.
3) European Comission, SETIS: Energy Efficiency and CO_2 Reduction in the Iron and Steel Industry, European comission, Brussels, (2015), 1.
4) World Steel Association: Worldsteel position paper, Steels Contribution to a Low Carbon Future and Climate Resilient Societies, World Steel Association, Brussels, (2017), 1.
5) J. C. M. Farla, C. A. Hendriks and K. Blok: *Clim. Change*, **29** (1995), 439.
6) K. Wang, C. Wang, X. Lu and J. Chen: *Energ. Policy*, **35** (2007), 2320.
7) D. Gielen and Y. Moriguchi: *Energ. Policy*, **30** (2002), 849.
8) M. Santen and M. Imris: Järnreduktionsprocess och anordning därför, Patent SE 536 291, (2013).
9) K. Harby, S. Chiva and J. L. Munoz-Cobo: *Exp. Therm. Fluid Sci.*, **53** (2014), 26.
10) G. N. Oryall and J. K. Brimacombe: *Metall. Trans. B*, **7B** (1976), 392.
11) J.-N. Tang, C. Tseng, N. Wang and W. Shyy: 49th AIAA Aerospace Sciences Meeting including the New Horizons Forum and Aerospace Exposition, American Institute for Aeronautics and Astronautics (AIAA), Reston, (2011), 1.
12) N. Huda, J. Nazer, G. Brooks, M. A. Reuter and R. W. Matusewicz: *Metall. Mater. Trans. B*, **43B** (2012), 1054.
13) E. O. Hoefele and J. K. Brimacombe: *Metall. Trans. B*, **10B** (1979), 631.
14) D. Geng, H. Lei and J.-C. He: *Metall. Mater. Trans. B*, **41B** (2010), 234.
15) H.-J. Odenthal, U. Thiedemann, U. Falkenreck and J. Schlueter: *Metall. Mater. Trans. B*, **41B** (2010), 396.
16) M. Bjurström, A. Tilliander, M. Iguchi and P. Jönsson: *ISIJ Int.*, **46** (2006), 523.
17) X. Zhou, M. Ersson, L. Zhong, J. Yu and P. Jönsson: *Steel Res. Int.*, **85** (2014), 273.
18) ANSYS 15.0 Fluent Theory Guide, ANSYS Inc., Canonsburg, (2013), 1.
19) F. Kerdouss, A. Bannari and P. Proulx: *Chem. Eng. Sci.*, **61** (2006), 3313.
20) P. Chen, J. Sanyal and M. P. Dudukovic: *Chem. Eng. Sci.*, **59** (2004), 5201.
21) M. K. Mondal and K. Logachander: *IJRET: Int. J. Res. Eng. Technol.*, **02** (2013), 451.
22) H. Odenthal, U. Falkenreck and J. Schlüter: Proc. European Conf. on Computational Fluid Dynamics (ECCOMAS CFD), Delft University of technology, Delft, (2006), 1.
23) A. Valencia, M. Rosales, R. Paredes, C. Leon and A. Moyano: *Int. Commun. Heat Mass Transf.*, **33** (2006), 302.
24) X. Zhou, M. Ersson, L. Zhong and P. Jönsson: *Steel Res. Int.*, **86** (2015), 1328.
25) R. Hong, H. Li, H. Li and Y. Wang: *Powder Technol.*, **92** (1997), 205.
26) B. Andersson, R. Andersson, L. Håkansson, M. Mårtenssen, R. Sudiyo, B. van Wachem and L. Hellström: Computational Fluid Dynamics for Engineers, Cambridge University Press, Cambridge, (2012), 1.